Available online at www.sciencedirect.com

SciVerse ScienceDirect

Ceramics International 39 (2013) 245–253

CERAMICS INTERNATIONAL

www.elsevier.com/locate/ceramint

Electrolytic deposition of fluorine-doped hydroxyapatite/ZrO_2 films on titanium for biomedical applications

Yong Huang[a], Yajing Yan[a], Xiaofeng Pang[a,b,*]

[a]*Institute of Life Science and Technology, University of Electronic Science and Technology of China, No.4 of Section 2, Jianshe North Road, Chengdu 610054, China*

[b]*International Centre for Materials Physics, Chinese Academy of Science, Shenyang 110015, China*

Received 9 May 2012; received in revised form 3 June 2012; accepted 4 June 2012
Available online 12 June 2012

Abstract

A novel method of electrolytic fluorine-doped hydroxyapatite/ZrO_2 double-layer coating was conducted on medical titanium in $ZrO(NO_3)_2$ aqueous solution and subsequently in the mixed solution of $Ca(NO_3)_2$, $NH_4H_2PO_4$ and NaF. The microstructure, phase composition, bond strength, dissolution rate and corrosion resistance of the films were studied. Results revealed that the additions of F^- reduced the crystallite and increased the crystallinity of hydroxyapatite, structure of apatite was changed from micro-petal-like crystals to nano-needle-like crystals, which aligned vertically to the substrate. The approximately 10 μm thick layers was much denser and uniform. Addition of ZrO_2 buffer layer could improve the bond strength between the fluorine-doped hydroxyapatite layer and the substrate. The bond strength of the double-layer coating was found to be significantly higher than that of pure hydroxyapatite coating even after soaking in normal saline for two weeks. In physiological solution, the double-layer coating showed lower dissolution rate and stronger corrosion resistance than pure hydroxyapatite coating.

Keywords: C. Corrosion; D. Apatite; D. ZrO_2; E. Biomedical applications

1. Introduction

The clinical implant must have excellent mechanical properties, good biocompatibility and corrosion resistance in the physiological environment. Titanium (Ti) substrates covered with hydroxyapatite ($Ca_{10}(PO_4)_6(OH)_2$, HAP) film have attracted much attention in the field of dentistry and orthopedics due to the integration of excellent mechanical performances of Ti and good biological activities of HAP [1–3]. The plasma spraying is widely used to prepare HAP film, but the thermal decomposition of HAP is inevitable owing to a high temperature handing is the serious problem of this approach [4]. Electrolytic deposition (ED) of HAP film has recently aroused widespread concern owning to many advantages of the technology such as a low temperature deposition process, the ease to control the film performance, the capacity to deposit on complicated surfaces, the usability and low price of device [5–7].

Nevertheless, HAP film prepared by current ED has two main disadvantages which could restrict the application potential of this method. On the one hand, the dissolution rate of HAP film is relatively high, which leads to disintegration of the film and makes the interface of bone and implant instability, thus hampers the fixation of HA-covered implants to the surrounding host tissues [8]. On the other hand, the poor bond strength (BS) between HAP and medical titanium has been a serious problem either during surgery or after implantation, owing to the great differences in thermodynamic properties between HAP and Ti substrate [9].

To avoid the above defects, two modifications have been studied of the current ED. First, NaF was added into the electrolyte to integrate F^- ions into the structure of the HAP crystals to get fluorine-doped hydroxyapatite ($Ca_{10}(PO_4)_6F_x(OH)_{2-x}$, FHAP, x is the degree of fluoridation)

*Corresponding author at: Institute of Life Science and Technology, University of Electronic Science and Technology of China, No.4 of Section 2, Jianshe North Road, Chengdu, Sichuan 610054 China. Tel./fax: +86 28 83202595.
E-mail address: pangxf2006@yahoo.com.cn (X. Pang).

0272-8842/$36.00
http://dx.doi.org/10.1016/j.ceramint.2012.06.017

coatings [8–11]. Fluorine is one of the microelement in the bone and tooth tissue of human, FHAP can resist physiological degradation much better than HAP [12,13], and it can also provide a adequately low fluoride dissolution rates to role in the cells and promote bone formation, while maintaining the relative biological activities [14,15]. Second, to enhance the BS of the HAP coating, an ED was used to get a double-layer coating (DLC) by introducing ZrO_2 layer as the transition between HAP and Ti substrate [16]. Yen et al. [17] reported that the outstanding adhesion was depended on the bonding of $Zr(OH)_4$ with OH bonds adsorbed on Ti substrate and OH bonds of HAP to constitute the very strong Ti–ZrO_2-HAP chemical bonding.

Therefore, the present work aims at preparing FHAP/ZrO_2 DLC by ED. It is hoped that the DLC electrodeposited using FHAP and ZrO_2 represent a good comprehensive effect to yield enhanced BS, physiological stability and corrosion resistance. The top-layer of functionality coating may provide good bioactive properties to accelerate bone healing, and the underlying transitional bond coat may be designed to achieve excellent BS. In the present work, the structural, electrochemical and mechanical behavior of the films was analyzed.

2. Materials and methods

2.1. Electrodeposition of FHAP/ZrO_2 films

Medical pure titanium sheets (Non-Ferrous Metals Ltd., Baoji, China) with a size of $10 \times 10 \times 0.9\ mm^3$ were used as substrates for ED. The sample surfaces were mechanically polished with SiC papers of different grits (400, 600, 800 and 1000), etched in 20% v/v of fluoric acid (HF) solution for 15 s, ultrasonically cleaned in ethyl alcohol and acetone for 600 s, rinsed in distilled water and finally dried at room temperature.

ED was carried out by electrochemical workstation (LK2005A, China). The titanium sheets were used as the working electrode, a Platinum foil ($15 \times 15 \times 0.1\ mm^3$) as the counter (auxiliary) electrode, and a saturated calomel electrode (SCE) as the reference electrode. First, the ZrO_2 coating was conducted in a electrolyte of 0.0625 M $ZrO(NO_3)_2$, at pH = 2.2 and a current density of $11.1\ mA/cm^2$ for 50 s, keeping the temperature at 25 °C. Then, the FHAP coating was conducted in a electrolyte composed of 0.042 M $Ca(NO_3)_2$, 0.025 M $NH_4H_2PO_4$ and 0.0008 M NaF, at pH = 4.0 and a current density of $0.9\ mA/cm^2$ for 1.5 h, keeping the temperature at 60 °C. After deposition, the samples were washed with deionized water, dried for 12 h and then annealed at 500 °C for 2 h in a vacuum environment (heating rate = 10 °C/min, cooling rate = 5 °C/min). For comparison, pure HAP coating, pure FHAP coating and HAP/ZrO_2 DLC were designated as control.

2.2. Coating characterization

Microstructure characterization of the deposit was analyzed by X-ray diffraction (XRD BEDE D1 SYSTEM) with Cu Kα radiation (40 kV, 30 mA) with a scanning speed of 1 °/min. The morphology was identified by scanning electron microscopy (SEM JSM-6490LV). Also an attached energy dispersive X-ray spectroscopy system (EDS GENESIS 2000 XMS) was used to analyze the chemical composition of the deposit. The deposit powder scrapped from the titanium surfaces was used in structure analysis conducted by fourier transform infrared spectroscopy (FTIR NICOLET NEXUS 670) using potassium bromide tablet technology. The thickness of films was measured using needle profilometer (Tencor Alpha-Step IQ).

2.3. Bond strength testing

An electronic universal testing machine (INSTRON-5567) was used to measure the BS between the apatite film and the substrate according to the ASTMF1044-05 international standard [8,18]. Before test, the coating surface ($10 \times 10\ mm^2$) was bonded to the metal surface with epoxy adhesive. The tensile test was carried out at a crosshead speed of 1 mm/min. For each testing material, there were six parallel samples whose average value was used to report the BS date. After BS test, cross-section examination of the coatings was studied by SEM-EDS system.

2.4. Dissolution testing

A tris-buffered normal saline solution (0.9% NaCl, pH 7.4, temperature 37 °C) was used to investigate the dissolution behavior of the layers. The covered electrode was immersed into the solution (without Ca^{2+} ions) for time periods of 1, 3, 5, 7, 9, 11 and 13 days. At the end of each soaking, the covered electrode was taken out and the concentration of Ca^{2+} dissolved from the films in the solution was detected with an inductively coupled plasma atomic emission spectrometer (ICP-AES; ICPS-100IV, SHIMADZU, Japan). An average of three measurements was taken for each sample. The BS between the apatite film and the substrate were measured after soaking in normal saline solution for time periods of 7 and 14 days, the test method is according with 2.3.

2.5. Electrochemical corrosion testing

The potentiodynamic polarization tests were conducted by electrochemical workstation (LK2005A, China). The working cell was a classical three electrodes cell in which platinum foil was used as counter (auxiliary) electrode, a saturated calomel electrode (SCE) as reference electrode and the uncovered or covered samples as working electrode with an exposed surface area of $1\ cm^2$. The polarization curves of the ZrO_2/FHAP-covered, HAP-covered and bare specimens in artificial saliva were obtained at a scan rate of 10 mV/s. The composition of the artificial saliva was [16]: NaCl (400 mg/l), KCl (400 mg/l), $CaCl_2 \cdot 2H_2O$ (795 mg/l), $NaH_2PO_4 \cdot H_2O$ (690 mg/l), KSCN (300 mg/l) and $Na_2S \cdot 9H_2O$ (5 mg/l), with the addition of lactic acid

to achieve a pH of 5. Before the start of the polarization tests, the samples were immersed into the artificial saliva for 20 min to obtain the stable open circuit potential.

2.6. Statistical analysis

All of the data were recorded as the mean ± standard deviations. Significant difference was analyzed by one-way variance analysis (ANOVA), subsequently calculated by the Student-Newman–Keuls post hoc test, and $P < 0.05$ was considered to be remarkable.

3. Results and disscussions

3.1. XRD analysis

The XRD profiles of the apatite covered samples are shown in Fig. 1. Typical apatite peaks were identified in all patterns (JCPDS file card #9-432). The intensity and resolution of FHAP diffraction peaks increased with the incorporation of F^- ions, which indicates that the DLC had smaller crystal size and higher crystallinity than HAP coating. As to FHAP/ZrO_2 DLC (Fig. 1a), the unusual strong peak at 25.9° was assigned to the diffraction line of FHAP at (002) plane, indicating a favored apatite crystal growth orientation along the c axis on the Ti substrate, it shows that the FHAP crystal aligned vertically to the substrate [14]. The classical main peak of crystal plane (21–30) seems to be restrained. In addition, the lattice constant α shifts between pure HAP and pure FA ($Ca_{10}(PO_4)_6F_2$), which is reflected by the typical crystal plane (3 0 0) [14], as can be seen from the magnified curve C in Fig. 1b, indicating the presence of FHAP crystal. No diffraction peak of ZrO_2 was observed, it might be due to the reason that ZrO_2 had not been transformed into crystalline phase.

3.2. FTIR analysis

After ED, the FTIR tests indicated phosphate formation (Fig. 2) of the Ti substrate covered with HAP and FHAP/ZrO_2. The bands at around 565 cm^{-1}–602 cm^{-1} are the bending vibration absorption peaks of the PO_4^{3-}, the bands at 633 cm^{-1} and 3571 cm^{-1} were corresponding with the wagging and stretching vibrations of the O–H group [8]. In addition, a significant change is that both the vibration number and the peak position changed, owing to the F^- ions joining into the channel structure, which could be explained by location group and factor group theory model [19]. The O–H band had three infrared activity vibration modes, separately corresponding to υ_1 (3571 cm^{-1}, stretching vibration), υ_2 (633 cm^{-1}, plane bending vibration) and υ_3 (716 cm^{-1}, in-plane bending vibration) [20]. The υ_2 and υ_3 amalgamated owing to the structural symmetry, so that merely υ_1 and υ_2 can be found in Fig. 2. When the F^- ions joined into the channel structures, the initial symmetry of vibrational modes had

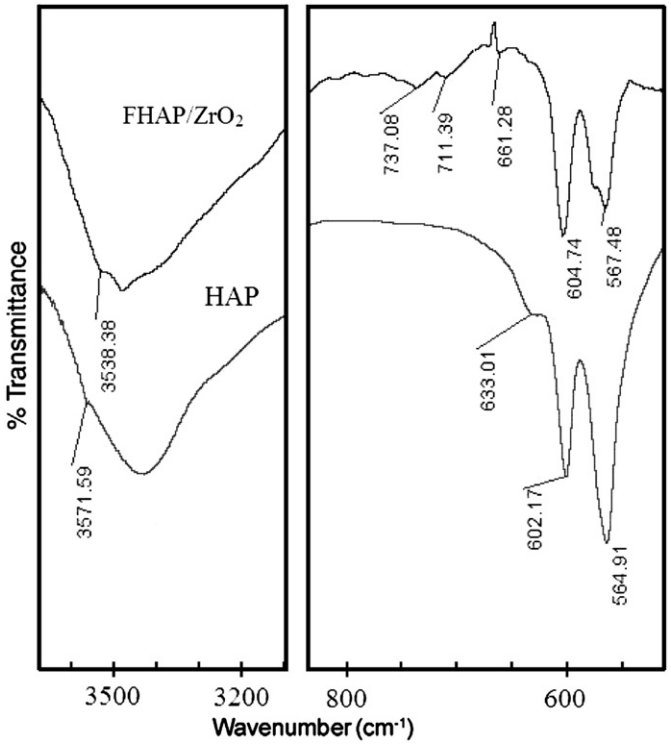

Fig. 2. FTIR spectra of deposits scraped from Ti substrate.

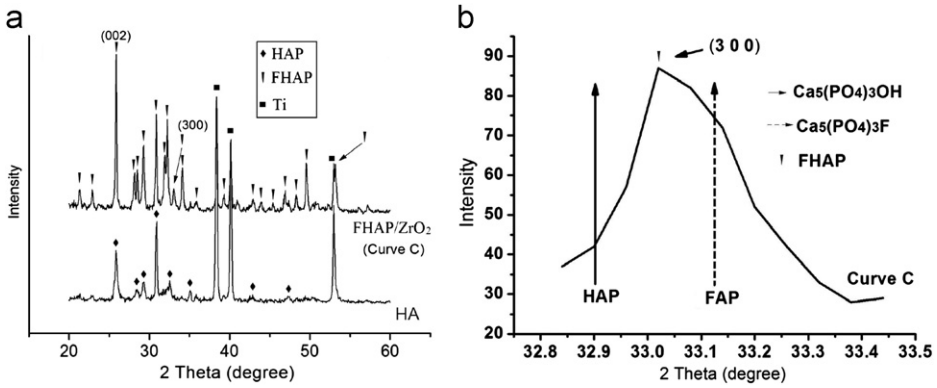

Fig. 1. (a) XRD patterns of HAP coating and FHAP/ZrO_2 double-layer coating on titanium (curve C) and (b) partial magnification of curve C.

been altered, leading to the disintegration of the initial merged vibrational mode and the appearance of new bands [21]. Owing to the appearance of OH–F band, the bond strength constants of OH^- declined, so that the υ_1' emerged in the low frequency location (3538 cm^{-1}). Remarkable electronegativity of F^- made the OH^- need the greater vibrational frequency to depart the bond axis, the result is that the $\upsilon_{2'}$ and $\upsilon_{3'}$ bending vibration emerged in the high frequency location (737 cm^{-1}, 711 cm^{-1} and 661 cm^{-1}) [20], as revealed in Fig. 2. The above results agree with the literature data by other researchers [8,9,14].

3.3. Morphology and chemical composition analysis of the films

The surfaces of the films are shown in Fig. 3(a and b). The HAP coating was characterized by individually resolvable HAP crystallites with a petal-like shape growing normal to the substrate surface. These petals fused together at one joint to construct the microporous structure with pore diameter being about 2 μm (Fig. 3a). The FHAP coating appeared different in that it was composed of nano-scaled apatite crystals in needle-like appearance and nano-pores formed between those nano-crystals (< 300 nm) (Fig. 3b). The crystallized needles aligned vertically to the substrate (Fig. 3b), this is in agree with the XRD results. The FHAP crystallites had a diameter less than 300 nm whose morphology is similar to that of HAP crystals in mature human dental enamel [22], bioactivity and osteoconductivity of coating could be further improved if coating materials were closer to bone mineral in crystal structure, size and morphology [23]. Note that these bio-ceramic films are prepared for promoting the generation of new bone on dental or orthopedic implanted prosthesis. The cross-section morphologies of the films are shown in Fig. 3c andd. Both the HAP and FHAPZrO_2 films formed smooth, uniform, approximately 10 μm thick layers on the Ti substrates without cracking or shedding at the interface.

EDS analysis explicitly illustrated the presence and proportion of calcium, phosphorus, oxygen, zirconium and fluoride, etc. in HAP and FHAP/ZrO_2 films as presented in Fig. 4a, b and c. The Ca/P atomic ratios of zone 0 (Fig. 4a) is about 1.53, a bit smaller than the standard 1.67. Therefore, the HAP coating is calcium deficient. As shown in Fig. 4b, the Zr/O atomic ratios of zone 1 is about 0.49 according to EDS, corresponding to ZrO_2 existing in the as-deposited layer, so this inner layer is ZrO_2 coating. The Ca/P atomic ratios for zone 2 (Fig. 4c) is about 1.49, a bit smaller than the standard 1.67. Therefore, the outer FHAP layer is also calcium deficient. It was reported that Ca-deficient apatite (Ca/P atomic ratios between 1.33 and 1.55) could be more beneficial to induce the formation of new bone in vivo [24]. Therefore, the Ca-deficient apatite coatings formed on ZrO_2 surface may benefit the formation of new bone in vivo. The degree of F substitution, x, for FHAP ($Ca_{10}(PO_4)_6(OH)_{2-x}F_x$) is about 1.0 according to the EDS results (Fig. 4c). It has been reported that the degree of fluoridation of $x \sim 1.33$ improves biomineralization in HA [25,26]. Savarino et al.'s study [27] suggested that the $Ca_{10}(PO_4)_3(OH)F$ coating was superior to both $Ca_{10}(PO_4)_3(OH)_2$ and $Ca_{10}(PO_4)_3F_2$ coatings in vivo.

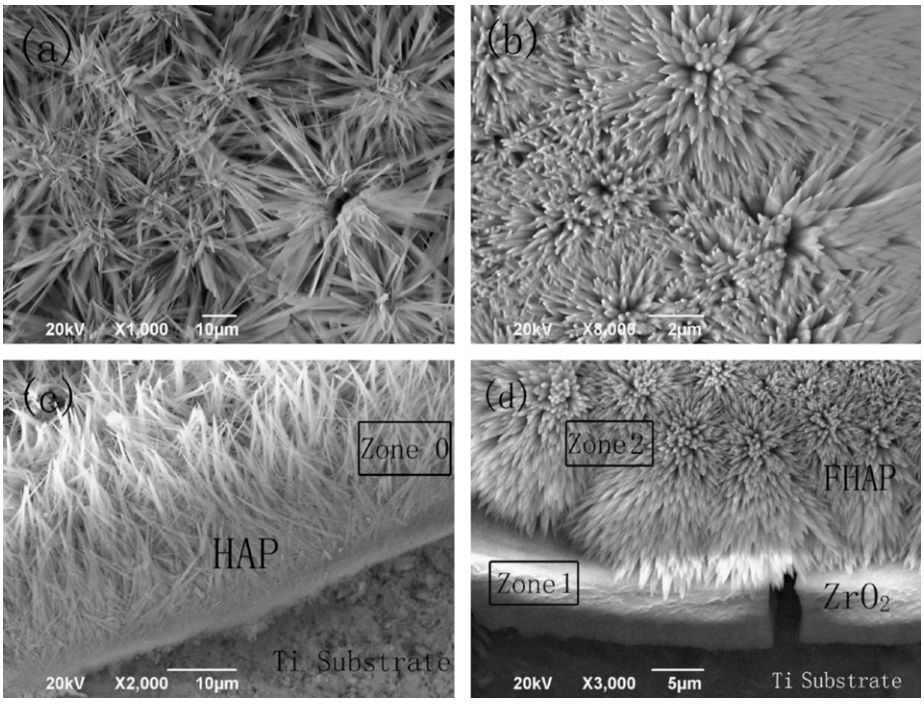

Fig. 3. SEM images of the prepared coatings on titanium: (a) surface morphology of the HAP film; (b) surface morphology of the FHAP/ZrO_2 films; (c) cross-section morphology of the HAP film and (d) cross-section morphology of the FHAP/ZrO_2 films.

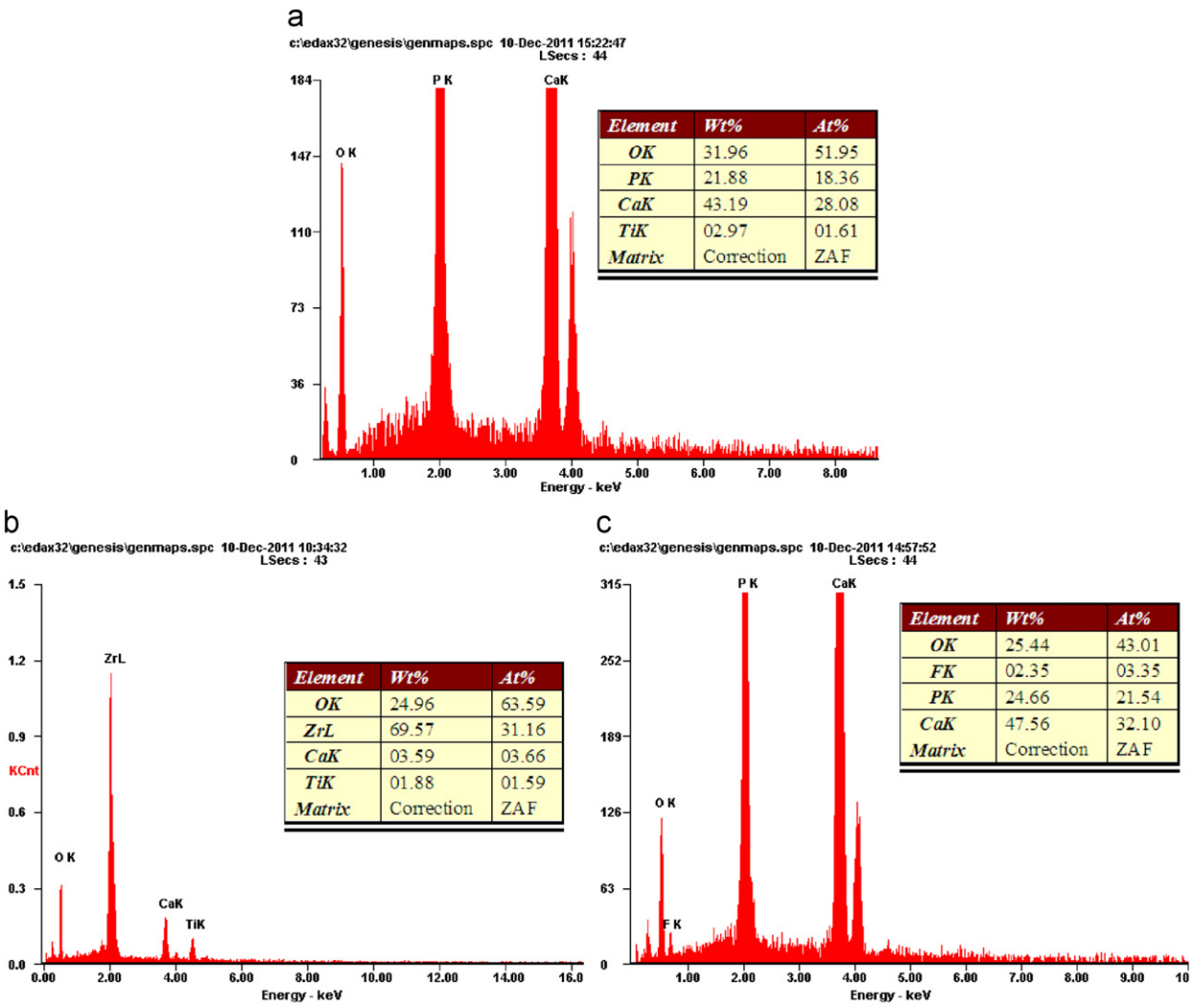

Fig. 4. EDS spectra of different zones: (a) Zone 0 of HAP coating; (b) Zone 1 of FHAP/ZrO_2 double-layer coating and (c) Zone 2 of FHAP/ZrO_2 double-layer coating.

In addition, Wang et al. [28] indicated that when the FHAP took the form of $Ca_{10}(PO_4)_6(OH)_{1.2\sim0.9}F_{0.8\sim1.1}$, that it could exhibit the best resistance to disintegration and the best bioactivity. F played an important role in influencing the physical and biological properties of the films [29].

3.4. Bonding strength evaluation

The BS of the coatings was measured by adhesion strength test accordance with ASTM standard F1044-05 [18]. In these tests, Pure HAP, FHAP and HAP/ZrO_2 films were designated as control. It has been a challenge to assess the BS of coatings with thin film. It is possible that the adhesive may infiltrate through the pores or cracks within the film and potentially bond to the substrate, thus affecting the effectiveness of test results. In the present study, the fracture interface of the covered specimens was examined by SEM-EDS in order to ensure that the fracture interface occurred within the apatite layers. According to the report [30], the BS of ZrO_2 with the substrate can reach 610 MPa, so the fracture interface of FHAP/ZrO_2 DLC should be within the inner FHAP layer.

BS of the apatite films to the Ti substrate is of the utmost importance for the biomedical applications to function properly in physiological environment. The BS results of the films are shown in Fig. 5. One-way ANOVA analysis and then hoc Student-Newman–Keul analysis exhibited significant differences within groups ($P<0.05$) and between each group ($P<0.05$), respectively. The BS measured of FHAP/ZrO_2 DLC was found to be ~26.2 MPa, far higher than the value of ~7.4 MPa of pure HAP film, while the value for FHAP film was ~13.4 MPa, and the value for HAP/ZrO_2 films was ~16.9 MPa. The pure HAP film exhibited the lowest BS, the BS of the FHAP and HAP/ZrO_2 films improved significantly compared to the HAP film. While the FHAP/ZrO_2 DLC exhibited still higher BS between the lamellae and the layer/substrate than that of either FHAP or HAP/ZrO_2 films, which may be due to several possible reasons. First of all, the cohesive strength between FHAP layer and substrate could be enhanced by adding ZrO_2 layer as intermediate transition coating [16]. It could be judged from previous research that the

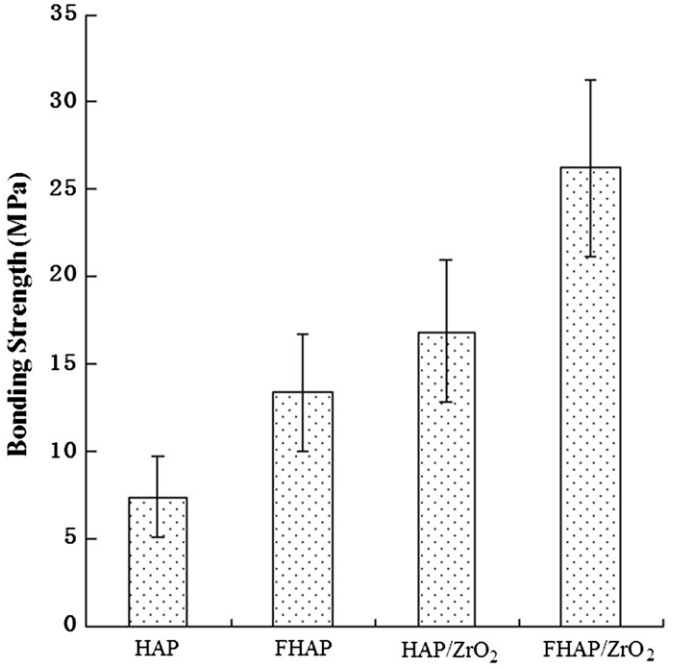

Fig. 5. Bond strength of all the coatings with respect to Ti substrate: (a) HAP coating, (b) FHAP coating, (c) HAP/ZrO_2 double-layer coating and (d) FHAP/ZrO_2 double-layer coating.

good adhesion was attributed to the bonding of $Zr(OH)_4$ with OH bonds adsorbed on Ti substrate and OH bonds of FHAP to form the extremely strong Ti–ZrO_2-FHAP chemical bonds [17]. Other factors of nano-needle-like film, such as decreased porosity and smaller FHAP crystal size certainly increasing the BS of the DLC [8,9]. Furthermore, with the doping of fluorine into HAP, the thermal expansion coefficient (TEC) decreased from 15×10^{-6}/°C to 9.1×10^{-6}/°C when HAP is completely changed into fluorapatite (FAP) [31], which is much closer to the TEC of ZrO_2 buffer layer (10.4×10^{-6}/°C) and the TEC of Ti substrate (8.6×10^{-6}/°C) [32]. Consequently, the doping of fluorine into HAP crystalline reduces the thermal mismatch and diminishes the residual stress within the layers, and thereby increasing the BS [31]. Finally, intricate P–O–F–Ca bonding may be generated in the transitional zone that helps enhance the BS; sintering heat treatment significantly improves spread of fluorine and oxygen and promoting activation for the chemical bonding procedure thus creating higher BS [31]. This BS value of FHAP/ZrO_2 films is higher than that of HAP film fabricated by traditional ED process (14 MPa) [3] and is close to that of fluorine-doped Ca–P films deposited on Ti reported by Wang et al. (26 MPa) [8,9]. Thus, it may be concluded that the FHAP/ZrO_2 films fabricated in this work has promising mechanical properties for using as an biomedical material in high load bearing environment.

3.5. Dissolution behavior analysis

An in vitro dissolution test was carried out to investigate the mechanical stability of the DLC when suffered from a similar physiological condition [33]. The dissolution

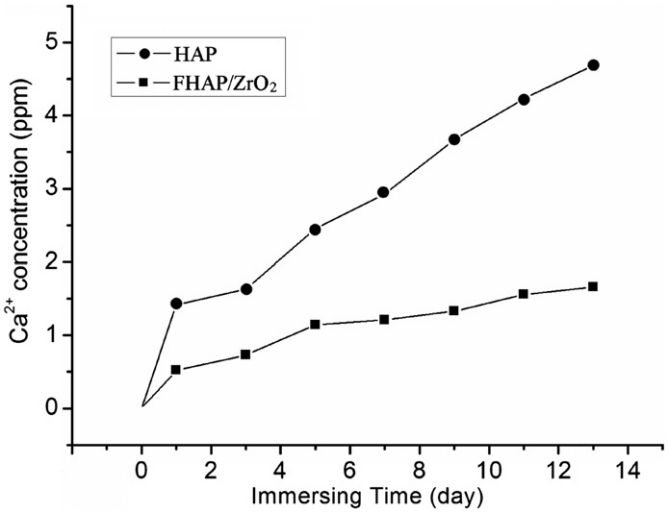

Fig. 6. Dissolution behavior of HAP and FHAP/ZrO_2 films.

behaviors of the films are shown in Fig. 6. The concentration of Ca^{2+} ions released from the films was investigated after soaking in the normal saline solution for up to 13 days. For all the samples, the dissolved amounts of Ca^{2+} ions increased with the extension of immersion time. At any moment, dissolution rate of the pure HAP coating is much more quickly than the FHAP/ZrO_2 DLC. Therefore, we may conclude that the FHAP/ZrO_2 DLC with doped F^- ions are more chemically stable in a physiological environment than HAP coating, owing to their denser apatite lattice structure and higher crystallinity [8].

The in vitro degradation studies have been investigated to assess the bonding durability of apatite-covered implants [34]. Following immersing in normal saline, the BS of DLC may degrade through physiochemical dissolution. The variation of BS of the films with the normal saline immersing duration is shown in Fig. 7. The values of BS of pure HA film are also listed for comparison. As can be discovered that after 1-week immersing, the BS decrease in the DLC was about 15.8%, while the decrease in the HAP film was found to be 87.8%. With increasing immerse duration, it is clear that the DLC shows a sustained decline up to the second week with a total of 31.6% drop in initial strength, while the HAP film has peeled off from the Ti substrate. After two weeks of immersing, only less serious deterioration in BS for DLC can be observed. The deterioration of BS comes mostly from the continuation of chemical dissolution of DLC, which undermines the bond of the lamella in the FHAP layer and the bond of the interface between apatite layer and ZrO_2 layer [35]. HAP coating has been shown to dissolve much faster, which leads to more bond decline at the interface of coating and substrate. As reported by previous studies, during immersion tests, unfortunately, many thin HAP films are heavily dissolved in short periods of time [34]. Ohtsuka et al.'s study [36] suggested that the amorphous HAP film nearly dissolved entirely within 1 day in Hanks' solution. Compared with pure HAP film,

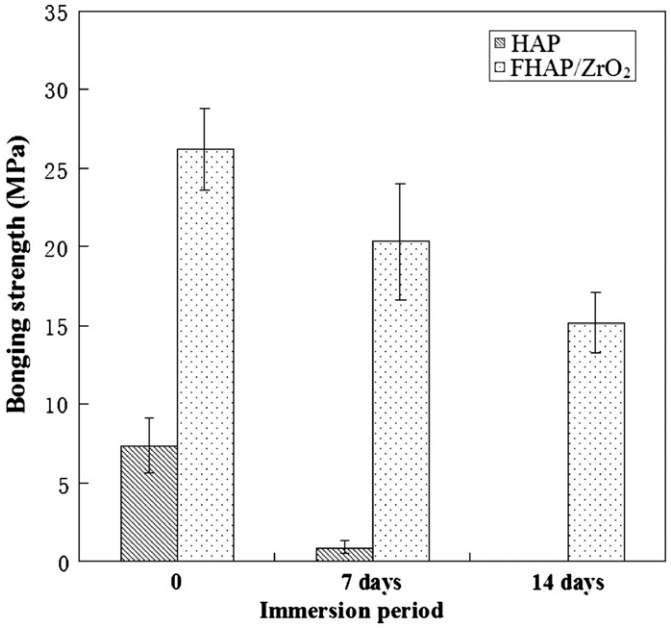

Fig. 7. Bond strength of HAP and FHAP/ZrO_2 films after immersion in normal saline solution.

the DLC dissolves much slower and hence the deterioration in BS for the DLC is significantly lower. This indicates that the FHAP/ZrO_2 DLC possess much superior physiostability and are less prone to deterioration of mechanical properties. The first two weeks is a key period for osteoblast adhesion and new bone formation after implantation. The analysis of the experiment shows that the compact nanostructured DLC covered Ti is stable enough, that could be used as a promising implant.

3.6. Electrochemical corrosion testing

In order to investigate the protection capacity of the films in physiological environment, the potentiodynamic polarization curves for the uncovered, HAP and FHAP/ZrO_2 covered Ti substrate samples in artificial saliva are shown in Fig. 8. The values of the corrosion potential (E_{corr}) and the corrosion current density (I_{corr}) were calculated from the curves and listed in Table 1. It was explicitly seen that entire curves moved towards the area of positive potential and lower current density.

It is widely accepted that I_{corr} could represent the corrosion rate of the metal surface [37]. In the present investigation, it was apparently observed from the curves that corrosion current density of the uncovered Ti sample was 207 nA/cm^2, I_{corr} of the uncovered HAP Ti sample was 37 nA/cm^2, and the I_{corr} of the uncovered FHAP/ZrO_2 Ti sample was 8 nA/cm^2, respectively. Covered Ti samples demonstrated lower corrosion current density, and the corrosion current density for the sample covered with pure HAP film was about 5 times lower than that of the uncovered sample. Moreover, the corrosion current density for the sample covered with FHAP/ZrO_2 films was

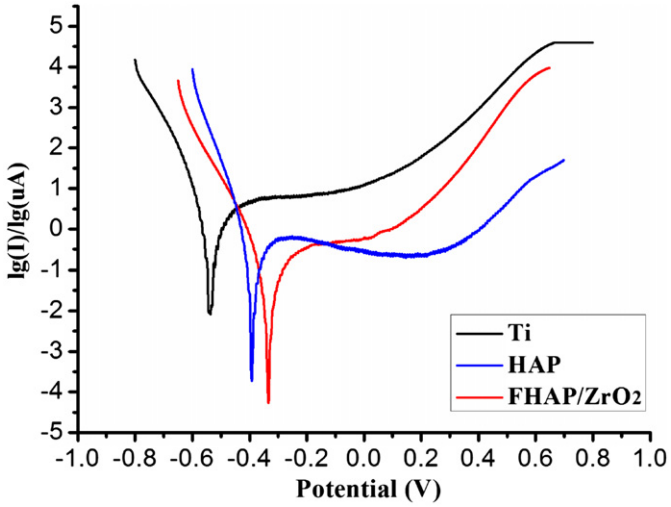

Fig. 8. Polarization curves in artificial saliva of the films on Ti substrate.

nearly 26 times lower than that of the uncovered sample. Since the I_{corr} values are directly proportional to the corrosion rate, obviously, Ti substrate covered with FHAP/ZrO_2 films can be considered to possess a good corrosion resistance, which lied from the formation of intensive microstructures when fluoride ions are introduced into the Ca–P crystal structure. The great difference indicates that the FHAP/ZrO_2 films can provide excellent protection for Ti implants. It was demonstrated by Hsu et al. [16] that the ZrO_2 inner film could provide effective protection for titanium substrate, even after the Ca–P film was completely dissolved owning to physiological corrosion effect.

3.7. Mechanism of electrolytic deposition

The mechanism of electrolytic deposition may be summarized as a series of electrochemical and chemical reactions. Firstly, electrolytic deposition of ZrO_2 coating from an aqueous solution of $ZrO(NO_3)_2$ may be summarized as follows [38]:

The three possible sources of OH^- at the cathode are

$$O_2 + 2H_2O + 4e^- \rightarrow 4OH^- \quad (1)$$

$$NO_3^- + H_2O + 2e^- \rightarrow 2OH^- + NO_2^- \quad (2)$$

$$H_2O + 2e^- \rightarrow H_2 + 2OH^- \quad (3)$$

The sequence of reactions leading to ZrO_2 oxide formation was considered to be the following:

$$ZrO(NO_3)_2 \rightarrow ZrO^{2+} + 2NO_3^- \quad (4)$$

$$ZrO^{2+} + H_2O \rightarrow Zr(OH)_2^{2+} \quad (5)$$

$$Zr(OH)_2^{2+} + 2OH^- \rightarrow Zr(OH)_4 \quad (6)$$

$$Zr(OH)_4 \rightarrow ZrO_2 + 2H_2O \quad (7)$$

Secondly, the formation process of fluorine-doped hydroxyapatite layer can be described by a combination

Table 1
Electrochemical parameters of the samples obtained from the polarization curves.

Sample	*Corrosion potential* E_{coor} (mV)	*Corrosion current density* I_{coor} (nA/cm^2)
Ti substrate	−541	207
HAP coating	−391	37
FHAP/ZrO_2 DLC	−338	8

of series reactions including acid-base reaction, precipitation reaction and crystallization process [14,39].

When a voltage is applied, the reaction processes at the surface of ZrO_2 film can be expressed as:

$$O_2 + 2H_2O + 4e^- \rightarrow 4OH^- \quad (8)$$

$$H_2O + 2e^- \rightarrow H_2 + 2OH^- \quad (9)$$

$$H_2PO_4^- + OH^- \rightarrow H_2O + HPO_4^{2-} \quad (10)$$

$$HPO_4^{2-} + OH^- \rightarrow H_2O + PO_4^{3-} \quad (11)$$

$$H_2PO_4^- + e^- \rightarrow HPO_4^{2-} + \frac{1}{2}H_2 \quad (12)$$

$$H_2PO_4^- + 2e^- \rightarrow PO_4^{3-} + H_2 \quad (13)$$

$$HPO_4^{2-} + e^- \rightarrow PO_4^{3-} + \frac{1}{2}H_2 \quad (14)$$

$$H_2PO_4^- \leftrightarrow HPO_4^{2-} + H^+ \quad (15)$$

$$HPO_4^{2-} \leftrightarrow PO_4^{3-} + H^+ \quad (16)$$

These reactions lead to the generation of hydrogen gas and hydroxyl ions. The increase in the concentration of hydroxyl ions leads to a local increase in pH values around the surface of ZrO_2 film. Witn F^- ions added into the electrolyte, the increased supersaturation of calcium phosphate may promote the formation of fluorine-doped hydroxyapatite [12], as follows:

$$10Ca^{2+} + 6PO_4^{3-} + xF^- + (2-x)OH^- \rightarrow Ca_{10}(PO_4)_6F_x(OH)_{2-x} \quad (17)$$

F–H bonds with adjacent OH^- along the c axis can be formed when F^- ions are doped, so the orientation of O–H in FHAP crystals is increased [40] and vertical FHAP crystals are produced, this is consistent with the previous XRD and SEM results.

4. Conclusions

Uniform and dense nanostructured FHAP/ZrO_2 DLC synthesized with ED, exhibit excellent mechanical and chemical integrity. The morphology of apatite was changed from micro-petal-like crystals to nano-needle-like crystals, and the coating was denser. The FHAP crystal was preferentially arranged in the (002) direction. A ZrO_2 base layer could act as a transition layer between FHAP layer and Ti substrate. The BS of the FHAP/ZrO_2 DLC was 354% larger than that of the HAP coating, which might result from collaborative effect of nanosized FHAP crystallites and the intermediate ZrO_2. The BS was found to diminish with normal saline soaking duration. However, the DLC exhibited superior mechanical stability, higher chemical stability and stronger corrosion resistance than the pure HAP film, indicating the much better long-term stability of the double-layer coating in physiological environment. The solid integrity of this DLC makes it a promising candidate for biomedical applications.

Acknowledgment

This work was supported by the National Basic Research Program of China (“973” Program, no. 2007CB936103). The authors thank Xuejiao Zhang for manuscript revision.

References

[1] H. Farnoush, L.A. Mohandesi, D.H. Fatmehsari, F. Moztarzaden, Modification of electrophoretically deposited nano-hydroxyapatite coatings by wire brushing on Ti–6Al–4V substrates, Ceramics International (2012), http://dx.doi.org/10.1016/j.ceramint.2012.02.079.
[2] S. Subramanian, D. MubarakAli, N. Thajuddin, Fabrication of corrosion resistant, bioactive and antibacterial silver substituted hydroxyapatite/titania composite coating on Cp Ti, Ceramics International 38 (2012) 731–740.
[3] Y. Han, T. Fu, J. Lu, K.W. Xu, Characterization and stability of hydroxyapatite coatings prepared by an electrodeposition and alkaline-treatment process, J, Journal of Biomedical Materials Research 54 (2001) 96–101.
[4] B.Y. Chou, E. Chang, Plasma-sprayed hydroxyapatite coating on titanium alloy with ZrO2 second phase and ZrO_2 intermediate layer, Surface and Coatings Technology 153 (2002) 84–92.
[5] P.C. Rath, L. Besra, B.P. Singh, S. Bhattacharjee, Titania/hydroxyapatite bi-layer coating on Ti metal by electrophoretic deposition: characterization and corrosion studies, Ceramics International 38 (2012) 3209–3216.
[6] L. Mohan, D. Durgalakshmi, M. Geetha, T.S.N. Sankara Narayanan, R. Asokamani, Electrophoretic deposition of nanocomposite (Hap+TiO_2) on titanium alloy for biomedical applications, Ceramics International 38 (2012) 3435–3443.
[7] D.Y. Lin, X.X. Wang, Preparation of hydroxyapatite coating on smooth implant surface by electrodeposition, Ceramics International 37 (2011) 403–406.
[8] J. Wang, C. Huang, Q. Wan, Y. Chen, Y. Chao, Characterization of fluoridated hydroxyapatite/zirconia nano-composite coating deposited by a modified electrocodeposition technique, Surface and Coatings Technology 204 (2010) 2576–2582.
[9] J. Wang, Y.L. Chao, G.B. Wan, H.P. Yan, Y.K. Meng, Fluoridated hydroxyapatite/titanium dioxide nanocomposite coating fabricated by a modified electrochemical deposition, Journal of Materials Science: Materials in Medicine 20 (2009) 1047–1055.
[10] X. Ge, Y. Leng, F.Z. Ren, X. Lu, Integrity and zeta potential of fluoridated hydroxyapatite nanothick coatings for biomedical applications, Journal of the Mechanical Behaviour of Biomedical Materials 4 (2011) 1046–1056.
[11] X. Ge, Y. Leng, B.C. Yao, S.L. Xu, R.K. Wang, F.Z. Ren, Antibacterial coatings of fluoridated hydroxyapatite for percutaneous implants, Journal of Biomedical Materials Research 95A (2010) 588–599.

[12] Y. Song, S.X. Zhang, J.N. Li, C.L. Zhao, X.N. Zhang, Electrodeposition of Ca–P coatings on biodegradable Mg alloy: in vitro biomineralization behavior, Acta Biomaterialia 6 (2010) 1736–1742.
[13] J.V. Rau, V.V. Smirnov, S. Laureti, A. Generosi, G. Varvaro, M. Fosca, Properties of pulsed laser deposited fluorinated hydroxyapatite films on titanium, Materials Research Bulletin 45 (2010) 1304–1310.
[14] J. Wang, Y.L. Chao, Q.B. Wan, Z.M. Zhu, H.Y. Yu, Fluoridated hydroxyapatite coatings on titanium obtained by electrochemical deposition, Acta Biomaterialia 5 (2009) 1798–1807.
[15] J.N. Li, Y. Song, S.X. Zhang, C.L. Zhao, F. Zhang, X.N. Zhang, In vitro responses of human bone marrow stromal cells to a fluoridated hydroxyapatite coated biodegradable Mg–Zn alloy, Biomaterials 31 (2010) 5782–5788.
[16] H.C. Hsu, S.C. Wu, C.H. Yang, W.F. Ho, ZrO_2/hydroxyapatite coating on titanium by electrolytic deposition, J, Journal of Material Science: Materials in Medicine 20 (2009) 615–619.
[17] S.K. Yen, S.H. Chiou, S.J. Wu, C.C. Chang, S.P. Lin, C.M. Lin, Characterization of electrolytic HA/ZrO_2 double layers coatings on Ti-6Al-4V implant alloy, Materials Science and Engineering C 26 (2006) 65–77.
[18] ASTM standard F 1044-05. ASTM International, West Conshohocken, PA.
[19] Q.X. Zhu, J.Q. Wu, Q.Q. Xu, Study on the tructure and thermal stability of hydroxyfluorapatite, Bulletin of Chinese Ceramic Society 27 (2008) 1119–1123.
[20] Q.X. Zhu, W.H. Jiang, H.D. Wang, C. Shao, Investigation on preparation factors for fluorhydroxyapatite by an aqueous precipitation method, Chinese Journal of Inorganic Materials 26 (2011) 1335–1340.
[21] G. Penel, G. Leroy, C. Rey, B. Sombret, J.P. Huvenne, E. Bres, Infrared and Raman microspectroscopy study of fluor-hydroxy and hydroxy-apatite powders, Journal of Material Science: Materials in Medicine 8 (1997) 271–276.
[22] D.Y. Lin, X.X. Wang, Y. Jiang, Effect of trisodium citrate on electrolytic deposition of hydroxyapatite coatings, Journal of Biomedical Materials Research Part B 96 (2010) 1–8.
[23] R. Narayanan, T.Y. Kwon, K.H. Kim, Direct nanocrystalline hydroxyapatite formation on titanium from ultrasonated electrochemical bath at physiological pH, Materials Science Engineering C 28 (2008) 1265–1270.
[24] S.V. Dorozhkin, A review on the dissolution models of calcium apatites, Progress in Crystal Growth and Characterization of Materials 44 (2002) 45–61.
[25] K. Cheng, W.J. Weng, H.B. Qu, P.Y. Du, G. Shen, G.R. Han, et al., Sol–gel preparation and in vitro test of fluorapatite/hydroxyapatite films, Journal of Biomedical Materials Research 69B (2003) 33–37.
[26] T.S. Wang, S. Zhang, X.T. Zeng, K. Cheng, M. Qian, W.J. Weng, In vitro behavior of fluoridated hydroxyapatite coatings in organic-containing simulated body fluid, Materials Science Engineering C 27 (2007) 244–250.
[27] L. Savarino, M. Fini, G. Ciapetti, E. Cenni, D. Granchi, N. Baldini, et al., Biologic effects of surface roughness and fluorhydroxyapatite coating on osteointegration in external fixation systems: an in vivo experimental study, Journal of Biomedical Materials Research Part A 66A (2003) 652–661.
[28] Y.S. Wang, S. Zhang, X.T. Zeng, L.L. Ma, W.J. Weng, W.Q. Yan, M. Qian, Osteoblastic cell response on fluoridated hydroxyapatite coatings, Acta Biomaterialia 3 (2007) 191–197.
[29] H.W. Kim, H.E. Kim, J.C. Knowles, Fluor-hydroxyapatite sol-gel coating on titanium substrate for hard tissue implants, Biomaterials 25 (2004) 3351–3358.
[30] S.K. Yen, M.J. Guo, H.Z. Zan, Characterization of electrolytic ZrO_2 coatings on Co–Cr–Mo implant alloys of hip prosthesis, Biomaterials 22 (2001) 125–133.
[31] S. Zhang, X. Zeng, Y. Wang, K. Cheng, W. Weng, Adhesion strength of sol–gel derived fluorinated hydroxyapatite coatings, Surface and Coatings Technology 200 (2006) 6350–6354.
[32] X.F. Xiao, R.F. Liu, Y.Z. Zheng, Hydoxyapatite/titanium composite coating prepared by hydrothermal–electrochemical technique, Materials Letters 59 (2005) 1660–1664.
[33] Y.W. Gu, K.A. Khor, P. Cheang, In vitro studies of plasma-sprayed hydroxyapatite/Ti-6Al-4V composite coatings in simulated body fluid (SBF), Biomaterials 24 (2003) 1603–1611.
[34] S.J. Ding, Properties and immersion behavior of magnetron-sputtered multi-layered hydroxyapatite/titanium composite coatings, Biomaterials 24 (2003) 4233–4238.
[35] Y.W. Gu, K.A. Khor, D. Pan, P. Cheang, Activity of plasma sprayed yttria stabilized zirconia reinforced hydroxyapatite/Ti–6Al–4V composite coatings in simulated body fluid, Biomaterials 25 (2004) 3177–3185.
[36] Y. Ohtsuka, M. Matsuura, N. Chida, M. Yoshinari, T. Sumii, T. Derand, Formation of hydroxyapatite on pure titanium substrates by ion beam dynamic mixing, Surface and Coatings Technology 65 (1994) 224–230.
[37] S. Hiromoto, M. Tomozawa, Hydroxyapatite coating of AZ31 magnesium alloy by a solution treatment and its corrosion behavior in NaCl solution, Surface and Coatings Technology 205 (2011) 4711–4719.
[38] S.K. Yen, The mechanism of electrolytic zro_2 coating on commercial pure titanium, Materials Chemistry and Physics 22 (2000) 256–262.
[39] N. Eliaz, M. Eliyahu, Electrochemical processes of nucleation and growth of hydroxyapatite on titanium supported by real-time electrochemical atomic force microscopy, Journal of Biomedical Materials Research Part A 80 (2007) 621–634.
[40] Y.M. Chen, X.G. Miao, Thermal and chemical stability of fluorohydroxyapatite ceramics with different fluorine contents, Biomaterials 26 (2005) 1205–1210.